Studying the effect of wall cooling in supersonic boundary layer flow using resolvent analysis

H. Jane Bae*
California Institute of Technology, Pasadena, CA 91125

Scott T. M. Dawson†
Illinois Institute of Technology, Chicago, IL 60616

Beverley J. McKeon‡
California Institute of Technology, Pasadena, CA 91125

Analysis of the resolvent operator is used to study the properties of high-speed turbulent boundary layers for cooled walls. Previous study [1] shows that the resolvent response modes in the relatively subsonic region of high-speed turbulent boundary layers with adiabatic wall boundary conditions follow the same scaling law as those of the incompressible boundary layer case, validating Morkovin's hypothesis on a mode-by-mode basis. Here, we study the effect of the cooled-wall boundary condition on the individual resolvent response modes to understand the underlying mechanisms that cause the failure of Morkovin's hypothesis and velocity transformations for increasingly non-adiabatic walls. In particular, we show that the density and temperature resolvent mode shapes for the cooled-wall case exhibit a secondary peak in the inner and logarithmic layer, which is a result of the non-monotonic mean temperature profile that is absent in adiabatic cases. We also show that the secondary peak becomes more prominent with decreasing surface temperature ratio. The deviation of the mean velocity profiles is attributed to the change in the response modes in the near-wall region, the effect of which is propagated further away from the wall through nonlinear interactions.

I. Nomenclature

x_1	=	streamwise location
x_2	=	wall-normal location
x_2^*	=	semi-local wall-normal location
x_2^c	=	wall-normal location of critical layer
x_3	=	spanwise location
δ	=	boundary layer thickness corresponding to the 99% of free-stream velocity
u_i	=	velocity component in the i direction
$\bar{u}_i$	=	mean velocity component in the i direction
$\bar{u}_1^+$	=	mean streamwise velocity profile in wall units
$\bar{u}_1^*$	=	mean streamwise velocity profile transformed as in Trettel and Larsson [2]
$\bar{u}_1^\star$	=	mean streamwise velocity profile transformed as in Bae et al. [1]
$\bar{u}_{1,\infty}$	=	free-stream streamwise velocity
$\bar{u}_{1,w}$	=	streamwise velocity at the wall
$(u_i)_1$	=	principal velocity response mode for velocity component in the i direction
u_τ	=	friction velocity
ρ	=	density
$\bar{\rho}$	=	mean density
$(\rho)_1$	=	principal density response mode
ρ_w	=	density at the wall

*Postdoctoral Scholar, Graduate Aerospace Laboratories, AIAA Member
†Assistant Professor, Mechanical, Materials and Aerospace Engineering, AIAA Member
‡Theodore von Karman Professor of Aeronautics, Graduate Aerospace Laboratories, AIAA Associate Fellow

ρ_∞ = free-stream density
T = temperature
$\bar{T}$ = mean temperature
$(T)_1$ = principal temperature response mode
T_w = wall temperature
T_r = recovery temperature
T_∞ = free-stream temperature
$\boldsymbol{q}$ = state vector (u_i, ρ, T)
μ = viscosity
$\bar{\mu}$ = mean viscosity
μ_w = viscosity at the wall
μ_∞ = free-stream viscosity
λ = second coefficient of viscosity
$\bar{\lambda}$ = mean second coefficient of viscosity
τ_w = wall shear stress
k = thermal conductivity
p = pressure
t = time
M_∞ = free-stream Mach number
M_τ = Mach number based on shear velocity and wall viscosity
$\overline{M}_\infty$ = relative Mach number to the free stream
$\overline{M}_w$ = relative Mach number to the wall
Re_δ = Reynolds number based on boundary layer thickness and free-stream quantities
Re_θ = Reynolds number based on momentum thickness and free-stream quantities
Re_τ = friction Reynolds number based on boundary layer thickness and wall (shear) quantities
Re_τ^* = semi-local friction Reynolds number
Pr = Prandtl number
c_p = specific heat at constant pressure
c_v = specific heat at constant volume
γ = ratio of specific heats, c_p/c_v
δ_{ij} = Kronecker delta
$\mathcal{R}$ = universal gas constant, $c_p - c_v$
$\mathcal{I}$ = identity matrix
$\mathcal{L}$ = linearized compressible Navier-Stokes operator
$\mathcal{H}$ = resolvent operator
$\boldsymbol{\psi}_j$ = resolvent response modes
$\boldsymbol{\phi}_j$ = resolvent forcing modes
σ_j = resolvent gains
$\boldsymbol{f}$ = nonlinear terms in the compressible Navier-Stokes equations
κ_1 = streamwise wavenumber
κ_3 = spanwise wavenumber
ω = temporal frequency
c = wave speed
r = recovery rate
E = total energy defined by the Chu [3] norm
E_K = turbulent kinetic energy
E_T = turbulent thermodynamic energy
E_{KK} = kinetic energy density of the principal response modes
E_{TT} = thermodynamic energy density of the principal response modes
$\hat{(\cdot)}$ = Fourier transformed quantities
$\breve{(\cdot)}$ = dimensional quantities
$(\cdot)^\dagger$ = conjugate transposed quantities
$(\cdot)^\intercal$ = transposed quantities

II. Introduction

The prediction of turbulent high-speed wall-bounded flows remains an active field of study for its technological importance in the aerospace industry. Given that the surface temperatures of supersonic and hypersonic flight vehicles are typically significantly lower than the adiabatic wall temperature due to considerable radiative cooling and internal heat transfer and that experiments for evaluating these vehicles are designed to have a non-adiabatic turbulent boundary layer at the wall, it is of practical importance to investigate wall-temperature effects on high-speed turbulent boundary layers.

Wall cooling causes a change in both the boundary-layer thickness and the fluid properties across the boundary layer. Many numerical studies have focused on the effect of wall cooling on the scaling of velocity fluctuations and the relationship between temperature and velocity fields [2, 4–11]. However, the literature is still limited due to the extremely long domain requirements needed to generate a fully developed state of the boundary layer as well as computational efforts to incorporate compressibility effects and avoid the formation of shocklets. Modeling the turbulent boundary layer with cooled walls is also a difficult challenge because, in particular, Morkovin's hypothesis [12] is known to fail for non-adiabatic wall temperatures, and the accuracy of the Van Driest transformation [13], as well as other proposed velocity transformations, deteriorate for increasingly non-adiabatic walls. There have been attempts to find a new scaling for compressible channel flows [2], which achieved an excellent collapse of the mean velocity profiles at different Reynolds and Mach numbers and wall heat transfer rates for high-speed channel flows. However, the same scaling does not provide a satisfactory collapse for turbulent boundary layers.

Studies over the past decade have demonstrated that the properties of the mean-linearized resolvent operator provide a framework with which to understand and predict the properties of incompressible wall-bounded turbulence [14–18]. Recent study of the compressibility effect using resolvent analysis demonstrated that the resolvent response modes can be useful in identifying the regions of significant difference in the different regimes of the Navier-Stokes equations on a mode-by-mode basis [1]. The study identified that the main source of the variation with respect to the incompressible case comes from the density variation in the wall-normal direction and the presence of Mach waves in the relatively supersonic region. This allowed the verification of Morkovin's hypothesis in the wave parameter space corresponding to the relatively subsonic region.

In the present work, we study the effects of wall cooling through the resolvent framework for compressible flows. Sec. III describes the resolvent formulation of the compressible Navier-Stokes equations. Sec. IV shows results from applying the formulation to supersonic boundary layers with cooled and adiabatic walls. Finally, conclusions are given in Sec. V.

III. Compressible Navier-Stokes equations

The non-dimensional compressible Navier-Stokes equations for a perfect gas are given by

$$\rho\left(\frac{\partial u_i}{\partial t}+u_j\frac{\partial u_i}{\partial x_j}\right)=-\frac{1}{\gamma M_\infty^2}\frac{\partial p}{\partial x_i}+\frac{1}{Re_\delta}\frac{\partial}{\partial x_j}\left[\mu\left(\frac{\partial u_i}{\partial x_j}+\frac{\partial u_j}{\partial x_i}\right)+\lambda\frac{\partial u_k}{\partial x_k}\delta_{ij}\right], \tag{1}$$

$$\frac{\partial \rho}{\partial t}+u_j\frac{\partial \rho}{\partial x_j}=-\rho\frac{\partial u_i}{\partial x_i}, \tag{2}$$

$$\begin{aligned}\rho\left(\frac{\partial T}{\partial t}+u_j\frac{\partial T}{\partial x_j}\right)=&-(\gamma-1)p\frac{\partial u_i}{\partial x_i}+\frac{\gamma}{PrRe_\delta}\frac{\partial}{\partial x_j}\left(k\frac{\partial T}{\partial x_j}\right)\\&+\gamma(\gamma-1)\frac{M_\infty^2}{Re_\delta}\mu\left[\frac{\partial u_i}{\partial x_j}\frac{\partial u_i}{\partial x_j}+\frac{\partial u_i}{\partial x_j}\frac{\partial u_j}{\partial x_i}+\lambda\left(\frac{\partial u_k}{\partial x_k}\right)^2\right],\end{aligned} \tag{3}$$

where the equations are given in nondimensionalized form using the Mach, Reynolds, and Prandtl numbers,

$$M_\infty=\frac{\breve{\breve{u}}_{1,\infty}}{\sqrt{\gamma\mathcal{R}\breve{T}_\infty}},\quad Re_\delta=\frac{\breve{\rho}_\infty\breve{U}_\infty\delta}{\breve{\mu}_\infty},\quad Pr=\frac{\breve{\mu}\,c_p}{\breve{k}}. \tag{4}$$

Here, we assume constant specific heat coefficients and constant Prandtl number, $Pr = 0.72$, and we set $\gamma = 1.4$ (diatomic gas).

Assuming a fully developed, locally parallel flow, the state variable $\boldsymbol{q} = [q_1, q_2, q_3, q_4, q_5]^\intercal = [u_1, u_2, u_3, \rho, T]^\intercal$ is

decomposed using the Fourier transform in homogeneous directions and time,

$$\boldsymbol{q}(x_1, x_2, x_3, t) = \iiint_{-\infty}^{\infty} \hat{\boldsymbol{q}}(x_2; \kappa_1, \kappa_3, \omega) e^{\mathrm{i}(\kappa_1 x_1 + \kappa_3 x_3 - \omega t)} \mathrm{d}\kappa_1 \mathrm{d}\kappa_3 \mathrm{d}\omega, \tag{5}$$

where $\hat{(\cdot)}$ denotes variables in the transformed domain, and the triplet $(\kappa_1, \kappa_3, \omega)$ is the streamwise and spanwise wavenumbers and the temporal frequency, respectively. The corresponding wave speed for each triplet is given by $c = \omega/\kappa_1$.

The mean turbulent state, $\bar{\boldsymbol{q}}(x_2) = [\bar{u}_1(x_2), 0, 0, \bar{\rho}(x_2), \bar{T}(x_2)]^\intercal$, corresponds to $(\kappa_1, \kappa_3, \omega) = (0, 0, 0)$ and is assumed to be known. Furthermore, with the parallel-flow assumption, which is reasonable as the base flow variations depend on the viscous time scale compared to the much faster convective time scale for fluctuations, the mean momentum equation (Eq. (1)) gives a constant $\bar{p}(x_2)$. In the remainder of the paper, we scale the pressure such that $\bar{p} = 1$ for simplicity.

The governing equations (Eqs. (1)–(3)) can be rewritten in the Fourier domain for each $(\kappa_1, \kappa_3, \omega) \neq (0, 0, 0)$ as

$$\begin{aligned}
&-\mathrm{i}\omega\hat{u}_i + \bar{u}_1\partial_1\hat{u}_i + \hat{u}_2\partial_2\bar{u}_i = -\frac{1}{\gamma M^2}\left(\partial_i\hat{T} + \bar{T}^2\partial_i\hat{\rho} + \hat{\rho}\bar{T}\partial_i\bar{T} + \bar{T}\hat{T}\partial_i\bar{\rho}\right) \\
&\qquad + \frac{\bar{T}}{Re}\left[\bar{\mu}\partial_j\left(\partial_j\hat{u}_i + \partial_i\hat{u}_j\right) + \bar{\lambda}\partial_i\left(\partial_j\hat{u}_j\right) + \frac{\partial\bar{\mu}}{\partial T}\partial_j\hat{T}\left(\partial_j\bar{u}_i + \partial_i\bar{u}_j\right)\right] + \hat{f}_i \qquad (6)\\
&-\mathrm{i}\omega\hat{\rho} + \bar{u}_1\partial_1\hat{\rho} + \hat{u}_2\partial_2\bar{\rho} = -\bar{\rho}\partial_i\hat{u}_i + \hat{f}_4 \qquad (7)\\
&-\mathrm{i}\omega\hat{T} + \bar{u}_1\partial_1\hat{T} + \hat{u}_2\partial_2\bar{T} = -(\gamma-1)\bar{T}\partial_i\hat{u}_i \\
&\qquad + \frac{\gamma\bar{T}}{PrRe}\left[\bar{\mu}\partial_j\partial_j\hat{T} + \frac{\partial^2\bar{\mu}}{\partial T^2}(\partial_2\bar{T})^2\hat{T} + 2\frac{\partial\bar{\mu}}{\partial T}\partial_2\bar{T}\partial_2\hat{T} + \frac{\partial\bar{\mu}}{\partial T}\partial_2^2\bar{T}\hat{T}\right] \\
&\qquad + \gamma(\gamma-1)\frac{M^2\bar{T}}{Re}\left[2\bar{\mu}\partial_2\bar{u}_1\partial_2\hat{u}_1 + 2\bar{\mu}\partial_2\bar{u}\partial_1\hat{u}_2 + \frac{\partial\bar{\mu}}{\partial T}(\partial_2\bar{u}_1)^2\hat{T}\right] + \hat{f}_5, \qquad (8)
\end{aligned}$$

where $\hat{\boldsymbol{f}}$ contains the nonlinear terms and $(\partial_1, \partial_2, \partial_3) = (\mathrm{i}\kappa_1, \mathrm{d}/\mathrm{d}x_2, \mathrm{i}\kappa_3)$. This can be equivalently expressed as

$$\hat{\boldsymbol{q}}(x_2; \kappa_1, \kappa_3, \omega) = [-\mathrm{i}\omega\mathcal{I} + \mathcal{L}(\kappa_1, \kappa_3, \omega)]^{-1}\,\hat{\boldsymbol{f}}(x_2; \kappa_1, \kappa_3, \omega), \tag{9}$$

where $\mathcal{L}$ is the linearized operator of the governing equations around the supersonic turbulent mean profile [19] and $\mathcal{I}$ is the identity matrix. The operator $\mathcal{H} = [-\mathrm{i}\omega\mathcal{I} + \mathcal{L}(\kappa_1, \kappa_3, \omega)]^{-1}$ is called the resolvent operator.

We take the singular value decomposition of the resolvent, namely,

$$\mathcal{H} = \sum_{j=1}^{\infty} \boldsymbol{\psi}_j(\kappa_1, x_2, \kappa_3, \omega)\sigma_j(\kappa_1, \kappa_3, \omega)\boldsymbol{\phi}_j^\dagger(\kappa_1, x_2, \kappa_3, \omega), \tag{10}$$

for $\sigma_j \geq \sigma_{j+1} \geq 0$ with the norm introduced by Chu [3] that eliminates pressure related energy transfer terms (compression work),

$$2E = (\boldsymbol{q}, \boldsymbol{q})_E = \|\boldsymbol{q}\|_E^2 = \int_0^{\infty}\left(\bar{\rho}u_i^\dagger u_i + \frac{\bar{T}}{\gamma\bar{\rho}M^2}\rho^\dagger\rho + \frac{\bar{\rho}}{\gamma(\gamma-1)\bar{T}M^2}T^\dagger T\right)\mathrm{d}x_2 \tag{11}$$

such that the orthogonality condition becomes

$$(\boldsymbol{\psi}_i(\kappa_1, x_2, \kappa_3, \omega), \boldsymbol{\psi}_j(\kappa_1, x_2, \kappa_3, \omega))_E = \delta_{ij}, \tag{12}$$

$$(\boldsymbol{\phi}_i(\kappa_1, x_2, \kappa_3, \omega), \boldsymbol{\phi}_j(\kappa_1, x_2, \kappa_3, \omega))_E = \delta_{ij}. \tag{13}$$

This norm has been used in numerous other studies of compressible flows where the definition of an inner product is required [e.g., 20–26]. The $\boldsymbol{\phi}_j$ and $\boldsymbol{\psi}_j$ form the right and left singular vectors for the forcing and velocity fields, and the real σ_j are the singular values. Here, we focus on the principal singular vectors, i.e. the principal forcing mode $\boldsymbol{\phi}_1$ and the principal response mode $\boldsymbol{\psi}_1 = [(q_1)_1, (q_2)_1, (q_3)_1, (q_4)_1, (q_5)_1]^\intercal = [(u_1)_1, (u_2)_1, (u_3)_1, \rho_1, T_1]^\intercal$, and the principal singular value σ_1.

Case	M_∞	M_τ	Re_τ	Re_θ	$\check{T}_w$, [K]	T_w/T_r	Reference
M4-R500-T100	4.0	0.10	505	5915	650	1.0	Bernardini and Pirozzoli [29]
M6-R450-T76	5.86	0.13	453	9455	300	0.76	Zhang et al. [30]
M6-R450-T25	5.84	0.17	450	2121	88	0.25	Zhang et al. [30]

Table 1 The free-stream Mach number M_∞, friction Mach number M_τ, friction Reynolds number Re_τ, Reynolds number based on momentum thickness Re_θ, the wall temperature T_w, and the surface temperature ratio T_w/T_r for the cases considered here.

IV. Resolvent analysis of cooled-wall supersonic boundary layers

We consider a flow over a flat plate with zero pressure gradient where the wall is cooled, i.e. the wall temperature is lower than the recovery temperature

$$T_r = T_\infty \left(1 + r(\gamma - 1)\frac{M_\infty^2}{2}\right), \tag{14}$$

where $r = Pr^{1/3}$ is the recovery rate. If the surface temperature ratio $T_w/T_r = 1$, where T_w is the temperature of the wall, the wall is adiabatic, whereas if $T_w/T_r < 1$, the wall is considered cooled. For the computation of the resolvent modes, we discretize in the wall-normal direction using a Chebyshev collocation method on a grid which is transformed by a rational transformation to increase resolution near the wall [27, 28]. The code has been validated in previous studies of compressible planar Couette flow and compressible turbulent boundary layers [1, 26].

A. Mean profiles

The turbulent mean profiles for the cooled-wall cases are obtained from Zhang et al. [30], where direct numerical simulations of a spatially evolving zero-pressure-gradient supersonic and hypersonic turbulent boundary layer with the wall temperature set below its nominally adiabatic value are computed. The results from the cooled-wall cases are compared against the results from an adiabatic wall boundary condition case with the mean profiles obtained from Bernardini and Pirozzoli [29]. In particular, the cooled wall cases under consideration are $M_\infty \approx 6$ with $T_w/T_r = 0.25$ and 0.76, and the adiabatic case is $M_\infty \approx 4$. In all cases, $Re_\tau = (\rho_w u_\tau \delta)/\mu_w \approx 450$–$500$. A tabulated list of cases considered is given in Table 1. Cases are named according to the nomenclature M[M_∞]-R[Re_τ]-T[$100T_w/T_r$].

We plot the transformed mean velocity profile in semi-local units and in defect form in 1(a,b), where the transformation in 1(a) is the one given by Trettel and Larsson [2],

$$x_2^* = \frac{\bar{\rho}(\tau_w/\bar{\rho})^{1/2}x_2}{\bar{\mu}}, \quad \bar{u}_1^* = \int_0^{\bar{u}_1^+} \left(\frac{\bar{\rho}}{\bar{\rho}_w}\right)\left(1 + \frac{1}{2\bar{\rho}}\frac{\mathrm{d}\bar{\rho}}{\mathrm{d}x_2}x_2 - \frac{1}{\bar{\mu}}\frac{\mathrm{d}\bar{\mu}}{\mathrm{d}x_2}x_2\right)\mathrm{d}\bar{u}_1^+, \tag{15}$$

and the one in 1(b) is given by Bae et al. [1],

$$\bar{u}_1^\star = \bar{u}_1^+ \left(\frac{\bar{\rho}}{\bar{\rho}_w}\right)^{1/2}, \tag{16}$$

which showed a satisfactory collapse for the outer region for adiabatic wall boundary conditions. We also plot the mean temperature profiles in 1(c,d). Note that, due to the normalized equation of state, the mean density profiles are the reciprocal of the mean temperature profile and thus omitted. As expected, the mean velocity profiles do not observe the same scaling laws as in the adiabatic case [30, 31]. While the overall scaling laws do not apply, the inner region for the velocity profile and the outer region for both the velocity and temperature profiles show reasonable collapse.

The lack of a universal scaling law for the mean profiles, as seen from the lack of collapse of the mean profiles in Figure 1, has implications for the resolvent modes. In Bae et al. [1], it was shown that the resolvent response modes for the supersonic boundary layer with adiabatic wall boundary conditions observe the same scaling laws as the incompressible boundary layer due to the collapse of the transformed mean velocity profile. In the absence of such scaling law, the universality of the resolvent modes will also break down (see Sec. IV.C). However, the mechanism that drives the deviation of the mean velocity profile from the classical incompressible counterpart can be identified by observing the wavenumber space in which the resolvent response modes deviate from their respective scaling law.

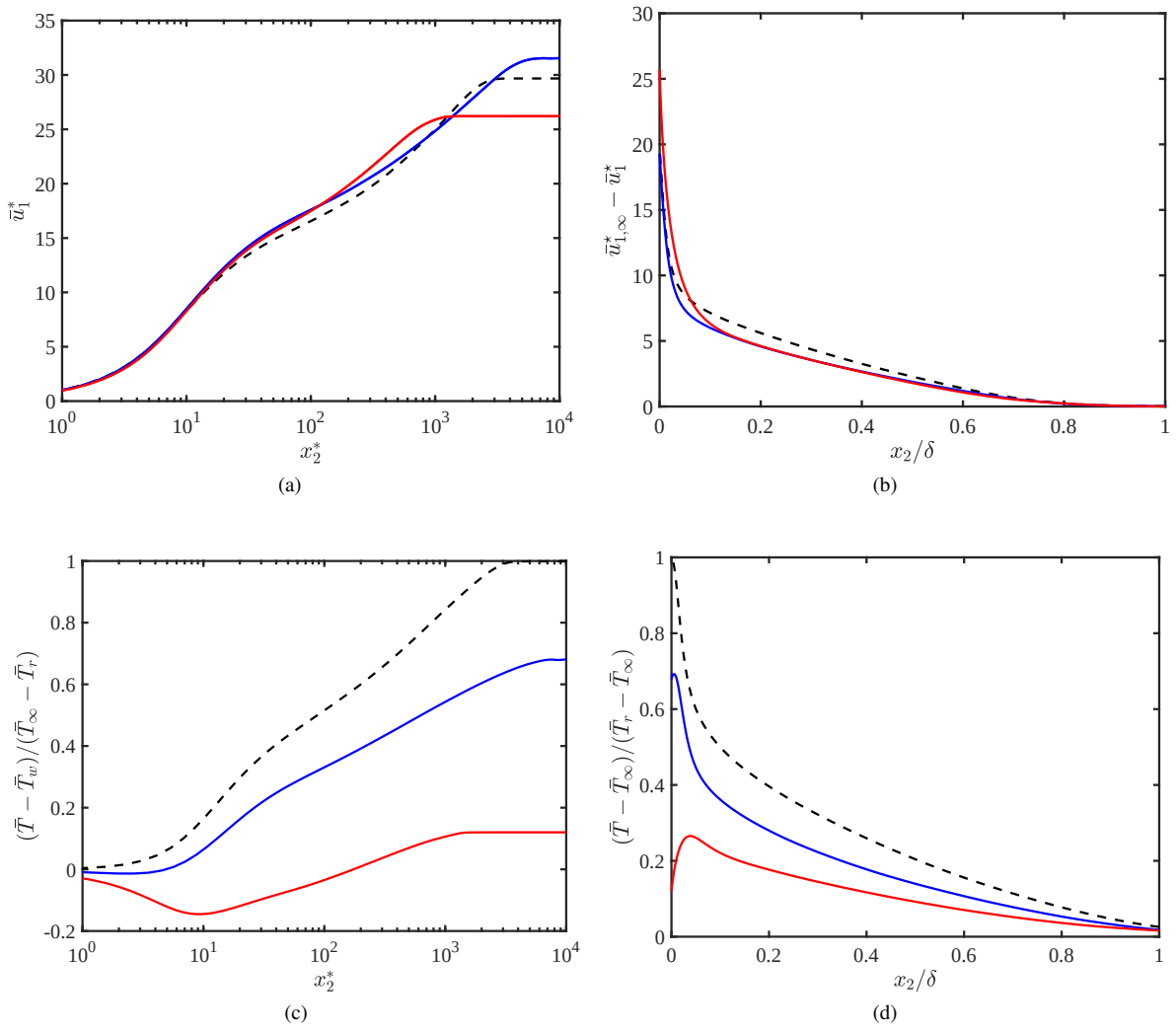

Fig. 1 Mean streamwise velocity profile (a) in semi-local units given by the transformation Eq. (15) and (b) in defect form given by the transformation Eq. (16). Mean temperature profile scaled by (c) the temperature at the wall and (d) the free-stream temperature. Lines are M4-R500-T100 (black dashed), M6-R450-T76 (blue) and M6-R450-T25 (red).

B. Effect of cooled walls on resolvent gains

The energy contribution of the principal mode to the total response subject to broadband forcing in the wall-normal direction can be quantified by $\sigma_1^2/\sum_j \sigma_j^2$. Figure 2 shows this energy contribution for the three cases under consideration for $x_2^{c+} \approx 15$, $x_2^c/\delta \approx 0.2$ and $x_2^c/\delta \approx 0.5$, where x_2^c is the critical layer where the wave speed matches the convective speed, i.e., $c = \omega/\kappa_1 = \bar{u}_1(x_2^c)$. Note that the energy contribution of unity signifies that the resolvent operator is rank-one while a low value indicates the operator is not low-rank.

Closer to the wall, at $x_2^{c+} \approx 15$, all three cases exhibit the presence of a relatively supersonic region, with the relative sonic line, $\overline{M}_\infty = 1$ clearly present, where the relative Mach number to the free stream is defined as

$$\overline{M}_\infty = \frac{(\kappa_1 \bar{u}_{1,\infty} - \omega) M_\infty}{(\kappa_1^2 + \kappa_3^2)^{1/2} \bar{T}_\infty^{1/2}}. \tag{17}$$

Although not shown, the resolvent response modes in the relatively supersonic region are centered around the sonic layer, where the convective velocity is equal to the relative sonic velocity [1]. Also, the irregular patterns shown in the relatively supersonic region are a numerical phenomenon and are attributed to the discrete representation of the

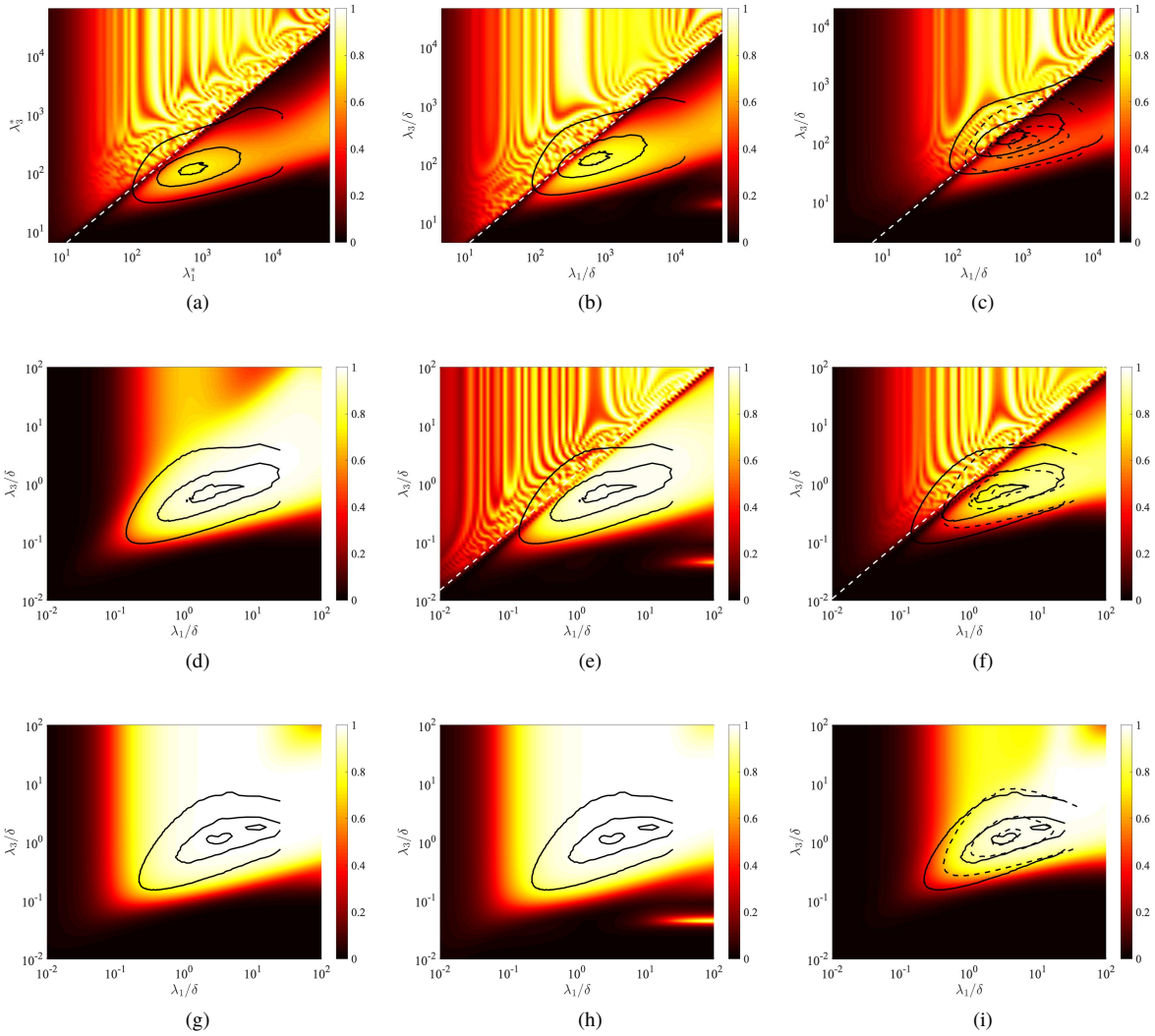

Fig. 2 Energy contribution of the principal mode to the total response subject to broadband forcing in the wall-normal direction for a given $(\kappa_1, \kappa_3, \omega)$ quantified by $\sigma_1^2 / \sum_j \sigma_j^2$ for (a,d,g) M4-R500-T100, (b,e,h) M6-R450-T76 and (c,f,i) M6-R450-T25 at critical layers corresponding to (a,b,c) $x_2^{c+} \approx 15$, (d,e,f) $x_2^c/\delta \approx 0.2$ and (g,h,i) $x_2^c/\delta \approx 0.5$. The contours are 10%, 50%, and 90% of the maximum energy of the premultiplied energy spectra for channel flow at $Re_\tau \approx 550$ (solid) and $Re_\tau \approx 180$ (dashed) [32] at the corresponding wall-normal locations. The white dashed line indicates the relative sonic line, $\overline{M}_\infty = 1$.

continuous acoustic modes [1, 26]. There may be a secondary relative sonic line located at $\overline{M}_w = -1$, where

$$\overline{M}_w = \frac{(\kappa_1 \bar{u}_{1,w} - \omega) M_\infty}{(\kappa_1^2 + \kappa_3^2)^{1/2} \bar{T}_w^{1/2}}, \tag{18}$$

for small values of $\bar{T}_w$ and $\kappa_1^2 + \kappa_3^2$ and large values of ω and M_∞; however, for the parameters considered in the present study, the secondary relative sonic line is not observed.

The behavior of resolvent gains in the three cases is similar, where, in the relatively subsonic region, the low-rank behavior aligns well with the high-energy region highlighted by the premultiplied energy spectra of the incompressible channel flow at $Re_\tau \approx 550$ [32]. The largest deviation is seen in the M6-R450-T25 case. Farther away from the wall, at $x_2^c/\delta \approx 0.2$, the higher Mach number cases still exhibit a relatively supersonic region. The relationship between the extent of the relatively supersonic region with Mach number is given in Eq. (17), and a three-dimensional

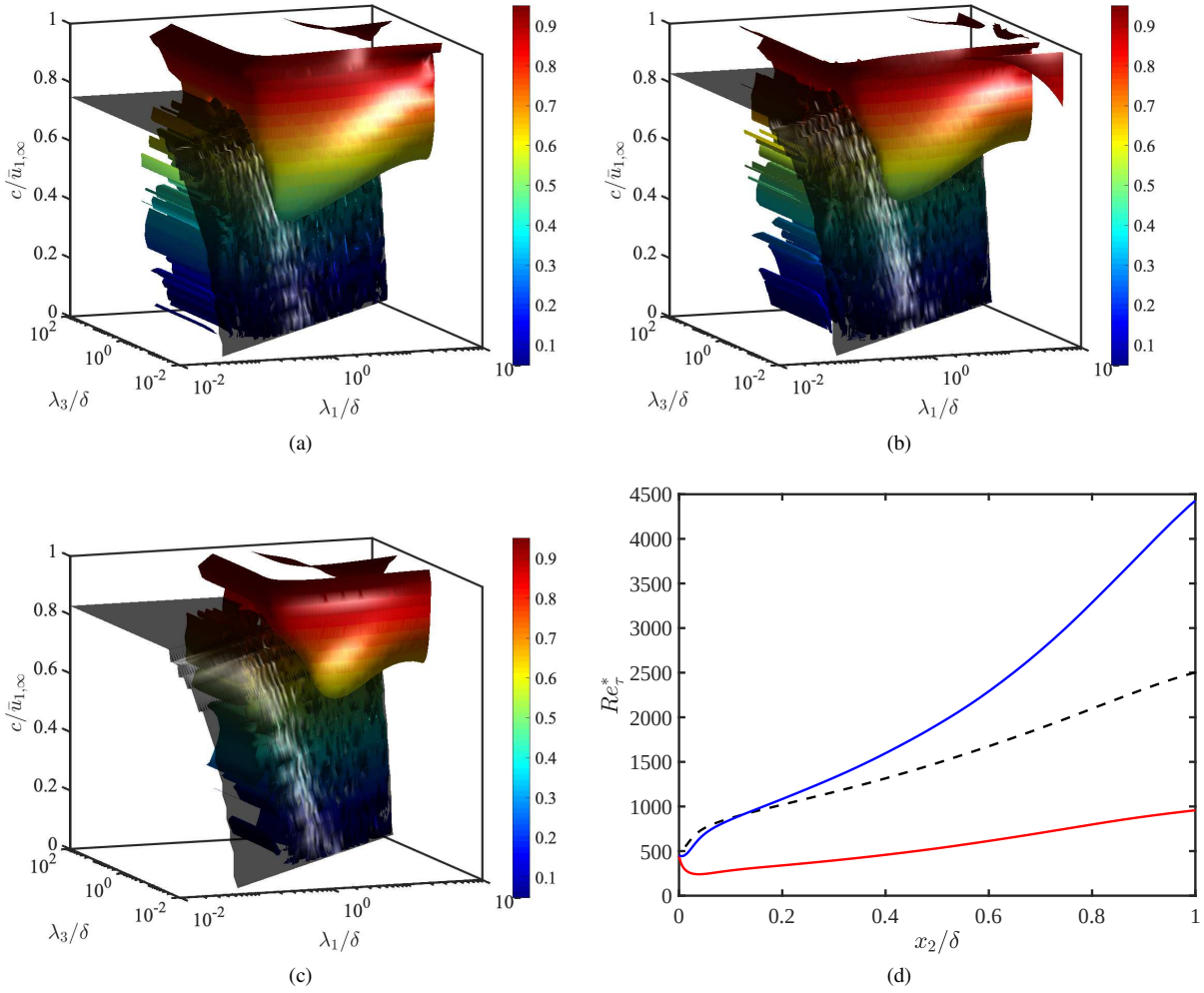

Fig. 3 Energy contribution of the principal mode to the total response subject to broadband forcing in the wall-normal direction for (a) M4-R500-T100, (b) M6-R450-T76 and (c) M6-R450-T25. The contour surface is $\sigma_1^2/\sum_j \sigma_j^2 = 0.75$ colored by wave speed c. The black surface indicates the relative sonic plane, $\overline{M}_\infty = 1$. (d) Semi-local Reynolds number as a function of wall-normal distance for M4-R500-T100 (black dashed), M6-R450-T76 (blue) and M6-R450-T25 (red).

depiction of this region can be seen along with the isosurface of the energy contribution of the principal mode in Fig. 3. It demonstrates an enlarged relatively supersonic region for the $M_\infty = 6$ cases. In both the wall-normal planes corresponding to $x_2^c/\delta \approx 0.2$ and $x_2^c/\delta \approx 0.5$, the behavior of the principal gain is similar in the relatively subsonic region for the M4-R500-T100 and M6-R450-T76 cases, whereas the energy contained in the principal mode is smaller for the M6-R450-T25 case.

The difference for the resolvent gains for M6-R450-T25 can be partly attributed to the differences in the semi-local Reynolds numbers, defined as

$$Re^*_\tau(x_2) = \frac{\bar{\rho}(x_2)(\tau_w/\bar{\rho}(x_2))^{1/2}\delta}{\bar{\mu}(x_2)}, \tag{19}$$

for the different cases (Fig. 3(d)). Up to $x_2^c/\delta \approx 0.5$, Re^*_τ for M4-R500-T100 and M6-R450-T76 are similar, whereas the Re^*_τ for the M6-R500-T25 case is significantly smaller. Bae et al. [1] showed that the meaningful Reynolds number for comparison of compressible resolvent modes is given by Re^*_τ, and given the large discrepancy between the semi-local Reynolds number, the difference in the energy spectra is not surprising. In contrast, the energy spectra of M6-R450-T25

Class	κ_1-scale	κ_3-scale	x_2-scale	c-scale	$(u_1)_1, (\rho)_1, (T)_1$-scale
Inner	$\frac{\kappa_1 \delta}{Re_\tau^*}$	$\frac{\kappa_3 \delta}{Re_\tau^*}$	x_2^*	c^*	$\widetilde{(q_i)}_1 \frac{1}{\sqrt{Re_\tau^*}}$
Outer	$\kappa_1 \delta Re_\tau^*$	$\kappa_3 \delta$	$\frac{x_2}{\delta}$	$\frac{c}{\bar{u}^\star_{1,\infty}}$	$\widetilde{(q_i)}_1$
Logarithmic	$\kappa_1 x_2^c x_2^{c*}$	$\kappa_3 x_2^c$	$\frac{x_2}{x_2^c}$	–	$\widetilde{(q_i)}_1 \sqrt{\frac{x_2^c}{\delta}}$

Table 2 Expected length scales for the universal modes of the resolvent operator for the turbulent boundary layer.

match better with the premultiplied streamwise energy spectra of a lower Reynolds number channel flow at $Re_\tau \approx 180$ [32] (see dashed spectra in Fig. 2(c,f,i)). Calibrating for this difference, the resolvent gains follow a similar behavior as the one observed in the adiabatic case.

C. Scaling of the principal response mode for cooled walls

As observed in Sec. IV.A, the mean streamwise velocity profiles for cooled walls do not collapse, even with semi-local variables, to the adiabatic boundary layer profile. This implies that the same scaling used in Moarref et al. [17] for the incompressible channel flow, which has been extended to adiabatic supersonic boundary layers [1], cannot be expected to work for the cooled wall cases. Nonetheless, we compare the resolvent response modes in order to identify points of discrepancy in the scaling laws; this will allow a modal assessment of the source of failure of Morkovin's hypothesis for cooled walls.

The universality and self-similarity of the resolvent scaling law for the incompressible channel flow [17], which have been subsequently extended to adiabatic supersonic boundary layers [1], are given in Table 2. We compare the resolvent response modes for various wave speeds in order to identify the region where the largest deviation from the adiabatic scaling law occurs. For comparison, the velocity response modes are normalized by the kinetic energy content in the response modes, and the temperature and density response modes are normalized by the thermodynamic energy. We define turbulent kinetic energy and turbulent thermodynamic energy as

$$E_K = (\boldsymbol{q}, \boldsymbol{q})_K = \int_0^\infty \bar{\rho} u_i^\dagger u_i \mathrm{d}x_2, \quad E_T = \int_0^\infty \frac{1}{\gamma M_\infty^2} \left(\frac{\rho^\dagger \rho}{\bar{\rho}^2} + \frac{T^\dagger T}{\bar{T}^2} \right) \mathrm{d}x_2, \tag{20}$$

respectively, and we normalize the velocity, density and temperature modes such that

$$\widetilde{(u_i)}_1 = \frac{\bar{\rho}^{1/2}(u_i)_1}{\sqrt{E_K}}, \quad \widetilde{(\rho)}_1 = \frac{(\rho)_1/(\gamma M_\infty^2 \bar{\rho}^2)^{1/2}}{\sqrt{E_T}}, \quad \widetilde{(T)}_1 = \frac{(T)_1/(\gamma M_\infty^2 \bar{T}^2)^{1/2}}{\sqrt{E_T}}. \tag{21}$$

In Fig. 4, the normalized resolvent response modes for streamwise velocity and temperature are given for the outer, logarithmic, and inner regions for the cases under consideration. The density mode shapes and amplitudes are identical to the temperature modes, and thus we omit them for brevity. We choose a set of modes in the outer region with $x_2^c/\delta = 0.7$, in the logarithmic region with $70 \leq x_2^{c*} \leq 100$, and in the inner region with $x_2^{c*} = 15$. The results from the cooled-wall cases are compared against the adiabatic case, which also collapses to the modes from the incompressible boundary layer [1]. We plot modes corresponding to a reference case of $Re_\tau^{ref} = 450$ and $(\kappa_1^{ref}, \kappa_3^{ref}) = (1, 10)$ with $c = \bar{u}_1(x_2^c)$ for each region. For example, we choose $\kappa_1 = \kappa_1^{ref} Re_\tau^* / Re_\tau^{ref}$ for the inner layer and $\kappa_1 = \kappa_1^{ref} Re_\tau^{ref} / Re_\tau^*$ for the outer layer.

As expected, the outer region modes in Fig. 4(a,b) collapse regardless of the surface temperature ratio, as the outer region mean velocity and temperature profiles still retain the scaling law observed for adiabatic cases as observed in Fig. 1(b,d). In all three regions, the velocity modes (Fig. 4(a,c,e)) show reasonable universal and self-similar behavior, with the M6-R450-T25 case in the inner region showing the most deviation, despite the lack of a universal scaling law for the mean velocity profiles. The largest deviation occurs in the temperature (and density) modes close to the wall (Fig. 4(f)), with increasing deviation with lower surface temperature ratios. In particular, the temperature modes develop a secondary peak closer to the wall, which becomes more prominent with smaller T_w/T_r and closer to the wall.

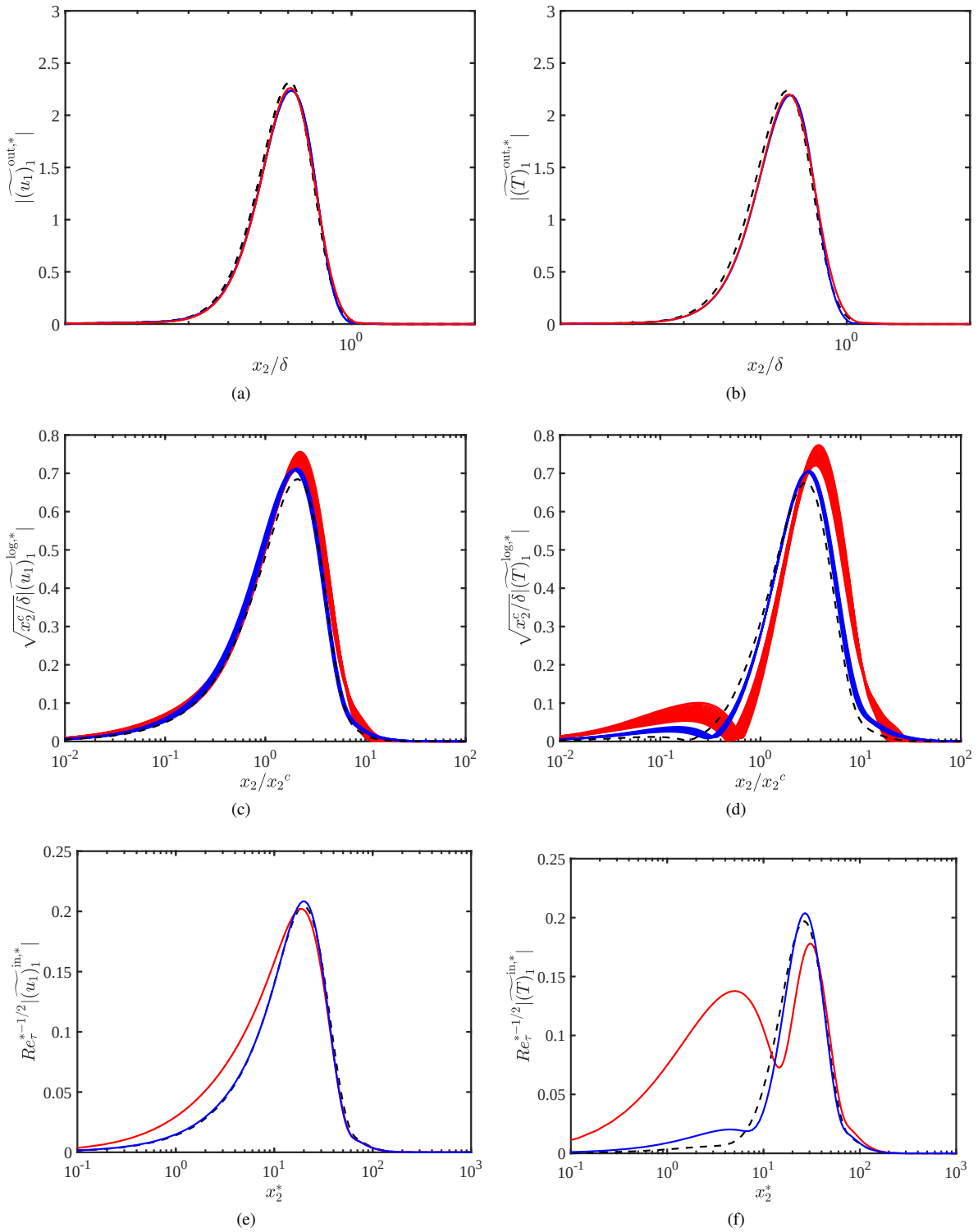

Fig. 4 Normalized resolvent response (a,c,e) streamwise velocity modes and (b,d,f) temperature modes for the (a,b) outer, (c,d) logarithmic, and (e,f) inner region. Lines are M4-R500-T100 (black dashed), M6-R450-T76 (blue) and M6-R450-T25 (red)

The satisfactory collapse of the modes in the logarithmic and outer layer could indicate that the changes observed in the mean profile stem from the modes closer to the wall, which propagates to the logarithmic region through nonlinear interactions.

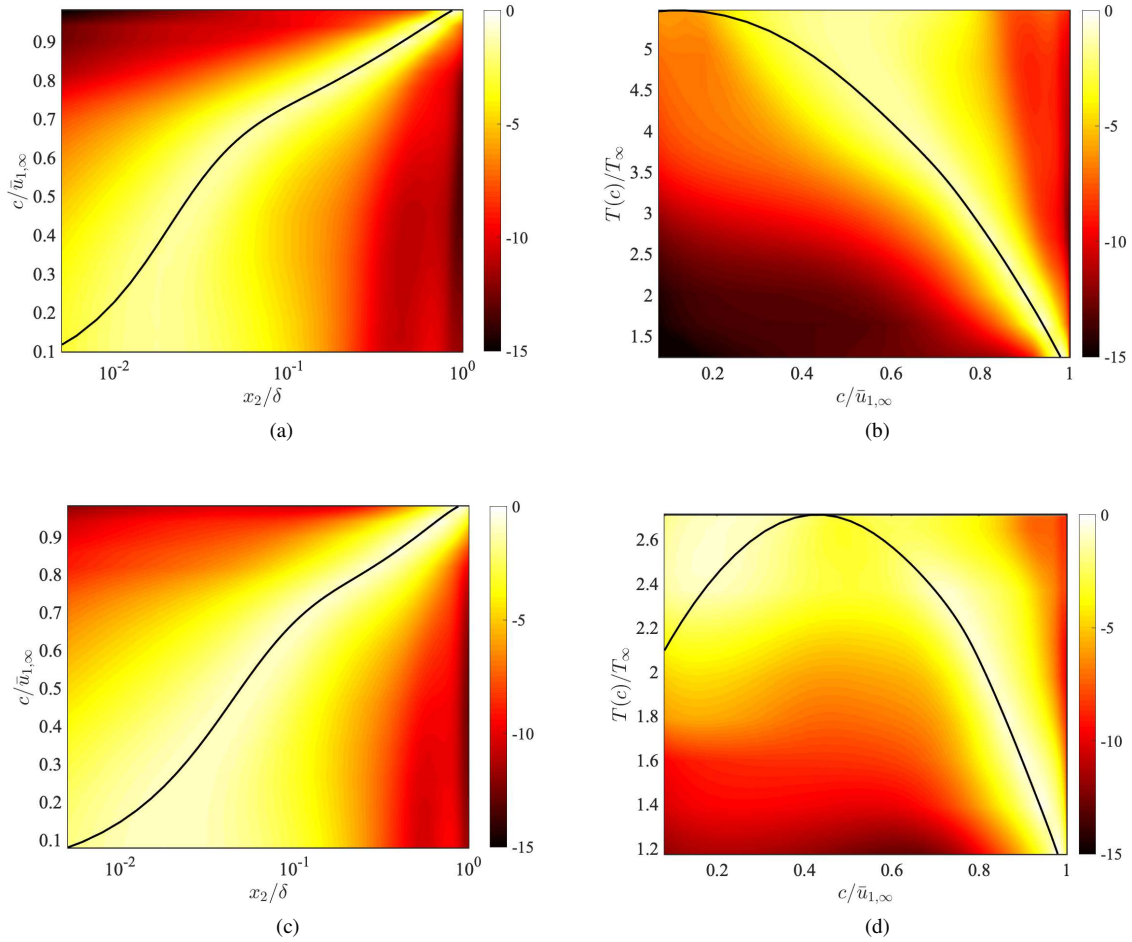

Fig. 5 Logarithm of the premultiplied one-dimensional (a,c) kinetic energy density $\log(E_{KK})$ and (b,d) thermodynamic energy density $\log(E_{TT})$ normalized by its maximum value at each c for the (a,b) M6-R450-T76 and (c,d) M6-R450-T25 cases conditionally sampled to $M_\infty < 1$. Solid lines indicate mean (a,c) velocity and (b,d) temperature profiles.

The formation of the secondary peak in the temperature and density modes can be explained by comparing the energy density of the thermodynamic response modes to the mean temperature profile. The premultiplied one-dimensional kinetic energy density of the principal velocity response modes is defined as

$$E_{KK}(x_2, c) = \sum_{i=1}^{3} \iint \kappa_1^2 \kappa_3 \left[\sigma_1(\kappa_1, \kappa_3, c)|\widetilde{(u_i)}_1|(\kappa_1, x_2, \kappa_3, c)\right]^2 \mathrm{d}\log\kappa_1 \mathrm{d}\log\kappa_3, \tag{22}$$

and the premultiplied one-dimensional thermodynamic energy density of the response modes is analogously defined as

$$E_{TT}(x_2, c) = \iint \kappa_1^2 \kappa_3 \left[\sigma_1(\kappa_1, \kappa_3, c)|\widetilde{(T)}_1|(\kappa_1, x_2, \kappa_3, c)\right]^2 + \left[\sigma_1(\kappa_1, \kappa_3, c)|\widetilde{(\rho)}_1|(\kappa_1, x_2, \kappa_3, c)\right]^2 \mathrm{d}\log\kappa_1 \mathrm{d}\log\kappa_3. \tag{23}$$

Note that the additional premultiplication by a factor of κ_1 is due to the fact that the energy intensity is defined as the integration of E_{KK} and E_{TT} over $c = \omega/\kappa_1$. We plot E_{KK} and E_{TT} normalized by its maximum value over x_2 for fixed

values of c in Fig. 5 for M6-R450-T76 and M6-R450-T25. For both cases, the principal resolvent modes are localized around the critical layer for the velocity profile. The thermodynamical energy density also shows localization of the principal temperature and density modes around the mean temperature profile. However, in the case of $T_w/T_r = 0.25$ case, due to the clear non-monotonic behavior in the temperature profile, there is a wide range of wave speeds c, $0 \leq c/\bar{u}_{1,\infty} \leq 0.75$, where two wall-normal locations have the same mean temperature corresponding to that of the critical layer. Thus, the localization of the temperature modes to the temperature corresponding to the critical layer causes the dual peak of response modes in the near-wall region, as observed in Fig. 4(d,f). While this behavior can be observed to a much lesser degree for the $T_w/T_r = 0.76$ case, the region in which the mean temperature profile is non-monotonic is significantly less than the $T_w/T_r = 0.25$ case, and the temperature mode resembles that of the adiabatic case.

V. Conclusions

The resolvent analysis framework has been applied to high-speed cooled-wall turbulent boundary layers. The wavenumber–frequency space can be divided into the supersonic and subsonic regions based on the relative Mach number similar to the adiabatic wall boundary case in Bae et al. [1]. While the mean velocity and temperature/density profiles lack a universal scaling even with transformation laws that are successful with adiabatic high-speed turbulent boundary layers, the resolvent velocity response mode shapes and amplitudes do coincide with its adiabatic and incompressible counterparts in the relatively subsonic region. The temperature and density response modes deviate close to the wall from the incompressible and compressible adiabatic wall cases. In particular, this discrepancy is expressed in the response modes through a formation of secondary peaks in the temperature and density modes, with the secondary peak amplitude becoming larger closer to the wall and with a smaller surface temperature ratio. The wave speeds in which the secondary peaks form are regions where the non-monotonic growth of the temperature profile leads to two wall-normal locations exhibiting the same temperature as the temperature of the critical layer. We also show that the two peaks observed align with these two wall-normal locations. This suggests that the main source of deviation between the adiabatic and the cooled-wall cases is the mean temperature profile, especially close to the wall, and the nonlinear interactions create the observed differences in the mean velocity profiles.

Acknowledgments

The authors acknowledge support from the Air Force Office of Scientific Research grant FA9550-16-1-0232.

References

[1] Bae, H. J., Dawson, S. T. M., and McKeon, B. J., "Resolvent-based study of compressibility effects on turbulent boundary layers," *J. Fluid Mech.*, 2020.

[2] Trettel, A., and Larsson, J., "Mean velocity scaling for compressible wall turbulence with heat transfer," *Phys. Fluids*, Vol. 28, No. 2, 2016, p. 026102.

[3] Chu, B.-T., "On the energy transfer to small disturbances in fluid flow (Part I)," *Acta Mech.*, Vol. 1, No. 3, 1965, pp. 215–234.

[4] Maeder, T., *Numerical investigation of supersonic turbulent boundary layers*, Vol. 394, ETH Zurich, 2000.

[5] Duan, L., Beekman, I., and Martin, M. P., "Direct numerical simulation of hypersonic turbulent boundary layers. Part 2. Effect of wall temperature," *J. Fluid Mech.*, Vol. 655, 2010, pp. 419–445.

[6] Shahab, M. F., Lehnasch, G., Gatski, T. B., and Comte, P., "Statistical characteristics of an isothermal, supersonic developing boundary layer flow from DNS data," *Flow Turbul. Combust.*, Vol. 86, No. 3-4, 2011, pp. 369–397.

[7] Chu, Y.-B., Zhuang, Y.-Q., and Lu, X.-Y., "Effect of wall temperature on hypersonic turbulent boundary layer," *J. Turbul.*, Vol. 14, No. 12, 2013, pp. 37–57.

[8] Zhang, Y.-S., Bi, W.-T., Hussain, F., and She, Z.-S., "A generalized Reynolds analogy for compressible wall-bounded turbulent flows," *J. Fluid Mech.*, Vol. 739, 2014, pp. 392–420.

[9] Hadjadj, A., Ben-Nasr, O., Shadloo, M. S., and Chaudhuri, A., "Effect of wall temperature in supersonic turbulent boundary layers: A numerical study," *Int. J. Heat Mass Transf.*, Vol. 81, 2015, pp. 426–438.

[10] Shadloo, M. S., Hadjadj, A., and Hussain, F., "Statistical behavior of supersonic turbulent boundary layers with heat transfer at $M_\infty = 2$," *Intl. J. Heat Fluid Flow*, Vol. 53, 2015, pp. 113–134.

[11] Zhang, C., Duan, L., and Choudhari, M. M., "Effect of wall cooling on boundary-layer-induced pressure fluctuations at Mach 6," *J. Fluid Mech.*, Vol. 822, 2017, pp. 5–30.

[12] Morkovin, M. V., "Effects of compressibility on turbulent flows," *Mécanique de la Turbulence*, Vol. 367, 1962, p. 380.

[13] Van Driest, E. R., "Turbulent boundary layer in compressible fluids," *J. Aeronaut. Sci.*, Vol. 18, No. 3, 1951, pp. 145–160.

[14] McKeon, B. J., and Sharma, A. S., "A critical-layer framework for turbulent pipe flow," *J. Fluid Mech.*, Vol. 658, 2010, pp. 336–382.

[15] Hwang, Y., and Cossu, C., "Linear non-normal energy amplification of harmonic and stochastic forcing in the turbulent channel flow," *J. Fluid Mech.*, Vol. 664, 2010, pp. 51–73.

[16] Sharma, A. S., and McKeon, B. J., "On coherent structure in wall turbulence," *J. Fluid Mech.*, Vol. 728, 2013, pp. 196–238.

[17] Moarref, R., Sharma, A. S., Tropp, J. A., and McKeon, B. J., "Model-based scaling of the streamwise energy density in high-Reynolds-number turbulent channels," *J. Fluid Mech.*, Vol. 734, 2013, pp. 275–316.

[18] McKeon, B. J., "The engine behind (wall) turbulence: perspectives on scale interactions," *J. Fluid Mech.*, Vol. 817, 2017.

[19] Mack, L. M., "Boundary-layer linear stability theory," AGARD Report No. 709, Part 3, NASA Jet Propulsion Laboratory, 1984.

[20] Hanifi, A., Schmid, P. J., and Henningson, D. S., "Transient growth in compressible boundary layer flow," *Phys. Fluids*, Vol. 8, No. 3, 1996, pp. 826–837.

[21] Malik, M., Alam, M., and Dey, J., "Nonmodal energy growth and optimal perturbations in compressible plane Couette flow," *Phys. Fluids*, Vol. 18, No. 3, 2006, p. 034103.

[22] Özgen, S., and Kırcalı, S. A., "Linear stability analysis in compressible, flat-plate boundary-layers," *Theor. Comp. Fluid Dyn.*, Vol. 22, No. 1, 2008, pp. 1–20.

[23] Malik, M., Dey, J., and Alam, M., "Linear stability, transient energy growth, and the role of viscosity stratification in compressible plane Couette flow," *Phys. Rev. E*, Vol. 77, No. 3, 2008, p. 036322.

[24] de Pando, M. F., Schmid, P. J., and Sipp, D., "A global analysis of tonal noise in flows around aerofoils," *J. Fluid Mech.*, Vol. 754, 2014, pp. 5–38.

[25] Bitter, N., and Shepherd, J., "Transient growth in hypersonic boundary layers," *7th AIAA Theoretical Fluid Mechanics Conference*, 2014, p. 2497.

[26] Dawson, S. T., and McKeon, B. J., "Studying the effects of compressibility in planar Couette flow using resolvent analysis," *AIAA SciTech*, 2019, p. 2139.

[27] Grosch, C. E., and Orszag, S. A., "Numerical solution of problems in unbounded regions: coordinate transforms," *J. Comput. Phys.*, Vol. 25, No. 3, 1977, pp. 273–295.

[28] Christov, C. I., "A complete orthonormal system of functions in $L^2(-\infty, \infty)$ space," *SIAM J. Appl. Math.*, Vol. 42, No. 6, 1982, pp. 1337–1344.

[29] Bernardini, M., and Pirozzoli, S., "Wall pressure fluctuations beneath supersonic turbulent boundary layers," *Phys. Fluids*, Vol. 23, No. 8, 2011, p. 085102.

[30] Zhang, C., Duan, L., and Choudhari, M. M., "Direct numerical simulation database for supersonic and hypersonic turbulent boundary layers," *AIAA J.*, Vol. 56, No. 11, 2018, pp. 4297–4311.

[31] Volpiani, P. S., Bernardini, M., and Larsson, J., "Effects of a nonadiabatic wall on supersonic shock/boundary-layer interactions," *Phys. Rev. Fluids*, Vol. 3, No. 8, 2018, p. 083401.

[32] Del Alamo, J. C., Jiménez, J., Zandonade, P., and Moser, R. D., "Scaling of the energy spectra of turbulent channels," *J. Fluid Mech.*, Vol. 500, 2004, pp. 135–144.